PNAS
www.pnas.org

Supplementary Information for

Architecture of DNA elements mediating ARF transcription factor binding and auxin-responsive gene expression in Arabidopsis

Alejandra Freire-Rios[1,2,*], Keita Tanaka[1,*], Isidro Crespo[3], Elmar van Wijk[1,4], Yana Sizentsova[5,6], Victor Levitsky[5,6], Simon Lindhoud[1], Mattia Fontana[1,4], Johannes Hohlbein[4,7], D. Roeland Boer[3], Victoria Mironova[5,6,#] and Dolf Weijers[1,#]

Corresponding authors: Victoria Mironova and Dolf Weijers
Email: victoria.v.mironova@gmail.com, dolf.weijers@wur.nl

This PDF file includes:

Supplementary text
Figures S1 to S8
Tables S1 to S5
Legends for Datasets S1 to S3
SI References

Other supplementary materials for this manuscript include the following:

Datasets S1 to S3

www.pnas.org/cgi/doi/10.1073/pnas.2009554117

Supplementary Text

Materials and Methods

Crystallization

The DNA-binding domain of AtARF1 was expressed and purified as previously described (1). The ARF1DBD-TGTCGG complex was prepared by mixing AtARF1DBD purified as previously described (1) in 20 mM Tris-HCl, 500mM NaCl buffer with an annealed dsDNA of sequence 5′-TTGTCGGCCTTTGGCCGACAA-3′ in a 1:1 molar stoichiometry, to a final protein concentration of 20 mg/mL. An initial crystallization hit (B10 condition of the Morpheus HT screen, Molecular dimensions [0.03M Sodium fluoride, 0.03M Sodium bromide, 0.03 M Sodium iodide, 0.05 M Tris (base), 0.05 M BICINE pH 8.5, 20% v/v Ethylene glycol; 10 % w/v PEG 8000]) was obtained using a full screen of the complex against sparse-matrix conditions. The diffraction data were obtained from crystals grown at 17 °C by hanging drop vapor diffusion of a 1:1 drop of the complex at 20 mg/mL protein concentration and crystallization buffer against 300 µl of crystallization buffer, 0.03 M Sodium fluoride, 0.03 M Sodium bromide, 0.03 M Sodium iodide, 0.05 M Tris (base), 0.05 M BICINE pH8.5, 20% v/v Ethylene glycol; 10 % w/v PEG 8000. Crystals were frozen in nylon loops by direct plunge freezing in liquid nitrogen. Data were collected in a single sweep at the XALOC beamline at the ALBA synchrotron (2). The crystals belonged to space group $P2_1$. Data were processed using the Global phasing AutoPROC program (3). The resolution was cutoff at 1.66 Å, see Table S1 for further statistics.

The structure was solved by molecular replacement using PHASER (4) from the CCP4 package (5). The structure was further refined using the program refmac v5.8.0230 (6), interspersed with manual adjustments using Coot (7). The model was validated and further adjusted and refined using the MolProbity web server (8). The final R and Rfree were 0.1717 and 0.1991, respectively. Further refinement statistics can be found in Table S1.

Analytical size exclusion chromatography

The DNA-binding domain of AtARF5 was expressed and purified as previously described (1). 500 pmol of each tested dsDNA was diluted in SEC buffer (15mM Hepes pH7.5, 150mM NaCl) to a final volume of 25 µL and each was injected on a Superdex 200 increase 5/150 (GE Healthcare) equilibrated in SEC buffer. For protein binding assays, a molar ratio of 2:1 (protein:DNA) were set in test tubes and incubated on ice for 1h, maintaining as final buffer the SEC buffer. 25 µL was injected in each case. For the apo-ARF control, the same amount of protein used for the assays was injected. The chromatography was run at 0.3ml/min on an ÄKTA Pure 25M and 280 and 260nm absorbance were recorded.

Analysis of genomic features of *TMO5* and *IAA11* promoters

We used ARF5 DAP-Seq peakset from Plant Cistrome Database (9). The data on conservation of promoter regions in 63 species from 7 lineages was taken from Plant RegMap database (10). DNase I digital genomic footprinting data from root tissues in (11) was taken from Plant RegMap (10). Building maps for *TMO5* and *IAA11* upstream regions was done using *base* and *Gviz* R packages.

Cloning and Mutagenesis

Cloning of all the DNA fragments used for testing the activity of *pTMO5*, *pTMO5∆1* and *pTMO5∆2* were done using the LIC method described in (12).
Mutagenesis of TMO5 AuxREs was done by overlap-extension PCR on the pTMO5-TMO5-3xGFP plasmid (13). The amplified fragments with mutated sites were replaced in the vector constructed in (14) using the XhoI and EcoRI unique restriction sites that flank the element.
To construct the plasmid for the wild-type and mutated *pIAA11*-driven *GFP* reporters, 3 kb of 5′-upstream region was amplified by PCR from Arabidopsis genomic DNA and inserted into pPLV4 using Seamless Ligation Cloning Extract (SLiCE). The mutations in *pIAA11∆1* were introduced by PCR-based method. The plasmid carrying *pIAA11∆2* was constructed through PCR using the *pIAA11∆1*-containing plasmid as template. Dataset S3 lists the primers used for the constructions.

Plant Materials and Growth Condition

All *Arabidopsis thaliana* plants used were from the Columbia-0 (Col-0) ecotype. After surface sterilization followed by dormancy breaking at 4°C for 48 hr–72 hr, seeds were grown at 22°C under long-day (16h light, 8h dark) condition on half-strength Murashige-Skoog (MS) medium. Plants for transformation or self-propagation were transferred to soil and grown under at 22°C under long-day condition.
To generate the lines in which TMO5-3xGFP was driven by the wild-type or mutated *pTMO5*, Col-0 plants were transformed with the plasmids (see Cloning and Mutagenesis) by floral dipping method using *Agrobacterium tumefaciens* strain GV3101. The lines in which n3GFP was driven by the wild-type or mutated *pIAA* were generated by transforming Col-0 by floral dipping method. These transformants were selected on half-strength MS media containing Kanamycin.
For preparing samples for the qRT-PCR to test auxin responsiveness of genes, 5 days-old seedlings grown with no antibiotics or exogenous hormone were transferred into MS media containing 2,4-Dichlorophenoxyacetic acid (2,4-D) (dissolved in DMSO) at a 1µM concentration, and then their roots were harvested at the appropriate time points. For each time point, mock groups were taken where seedlings have been transferred to MS containing DMSO.
For testing the auxin response of the *pIAA11WT-, pIAA11∆1-* and *pIAA11∆2-n3GFP* reporter lines, 5-day-old seedlings were transferred into MS media containing1µM 2,4-D and incubated for 6 hr.

Phenotypic complementation assay

The lines that express TMO5-tdT driven by *pTMO5*, *pTMO5∆1* and *pTMO5∆2* in the *tmo5 t5l1* double mutant (14) background were generated by introducing the transgenes into *tmo5*/*tmo5 T5L1*/*t5l1* plants by floral dipping and collecting the progeny of the self-fertilized plants. Phosphinothricin was used for the selection of transformants. The background genotypes were determined based on PCR as well as phenotypes of siliques and roots.
To analyze the vascular pattern of the lines, the T_4 generation seeds were vernalized for three days at 4°C, then germinated and grown for seven to eight days on half-strength MS media containing phosphinothricin and carbenicillin. The protoxylem tissue in primary roots of the seedlings were observed under a stereoscopic microscope.

Meta-analysis of auxin responsive transcriptomes

We analyzed all available datasets taken from *Arabidopsis thaliana* after auxin exposure (40 in total). After filtering out those with insufficient number of differentially expressed genes (less than 100 up or downregulated genes), this left us 5 RNA-Seq datasets and 10 microarray datasets (15–22). For further details see Table S3. Upstream regions [-1500;+1] of protein-coding genes were retrieved using R package *biomaRt* (23). 21098 genes were taken into meta-analysis of microarray data and 27628 genes for RNA-Seq data. Association between the presence of a particular AuxRE repeat with a transcriptional response to auxin was done with *metaRE* R package (24). For each dataset, the portion of auxin (up/down)regulated genes having a particular element versus all auxin-regulated genes was compared with the portion of auxin not (up/down)regulated genes with the element versus whole list of not (up/down)regulated genes. Comparison was done by Fisher's exact test, individual p-values were combined into meta-p-values by Fisher's method and adjusted with FDR Benjamini-Hochberg multiple testing procedure.

Quantitative RT-PCR analysis

Primers were designed using Beacon Designer 8 software (Premier Biosoft International). RNA isolation was done with TRIzol Reagent (Invitrogen) and the RNeasy kit (Qiagen). cDNA was prepared with the iScript cDNA Synthesis kit (BioRad) according to the protocol provided by the manufacturer. qRT-PCR reactions were performed with iQ SYBR Green Supermix (BioRad) and run in a CFX384 Real-Time PCR detection system (BioRad). Reactions were done in triplicate with two biological replicates. Data were analyzed in Rstudio, the gene expression levels were log2 transformed and normalized relative to ACT, CDKA1.1 and EEFa4. One-way ANOVA with Tukey post-hoc test and two-way ANOVA methods were applied to identify statistical significant changes. All the primers used for qRT-PCR are listed in Dataset S3.

Microscopy and fluorescent signal quantification

All the root confocal imaging was done in the Leica SP5 II system (HyD detector) microscope with 20× numerical aperture (NA) = 0.75 and 63× NA = 1.20 water-immersion objective and pinhole equivalent to 1.0× the Airy disk diameter. Roots were stained with a 10 µg/ml solution of Propidium Iodide (PI). TMO5-3GFP was excited at 488 nm, and its fluorescence was detected at 498–530 nm. The n3GFP driven by the wild-type and mutated *pIAA11* were excited at 488 nm and detected at 500 nm–525 nm.

Fluorophore intensities were measured using the LAS-AF 2.6.3 software (Leica Microsystems CMS GmbH). Acquisition settings were set on the brightest sample and kept for all the samples. The relative average pixel intensities were measured using the same region of interest in all samples.

smFRET-based protein-DNA binding analysis

DNA-binding domains of AtARF1 and AtARF5 were expressed and purified as previously described (1). The measurements were performed as described in (25). Briefly, labelled dsDNA oligos (IR8-donor [5'-ACTCTTTTTTGTCGGggaaaaggCCGACAATCCGTGTG-3'] / IR8-acceptor [5'-CACACGGATTGTCGGcctttccCCGACAAAAAAGAGT-3'] and DR5-donor [5'-ACTgCcTTTTGTCGGccttTGTCGGATCCGTGTG-3'] / DR5-acceptor [5'-CACACGGATCCGACAaaaggCCGACAAAAgGcAGT-3']; Green nucleotide is labeled with Cy3 and red nucleotide is labeled with ATTO647N; AuxRE's are underlined on forward strand) were immobilized to a PEGylated glass coverslip through a neutravidin bridge, inside the well of a silicone gasket. Each titration was performed with increasing concentrations of purified AtARF1-

DBD and AtARF5-DBD proteins in a single well, washing it between data points with ~600 μL of PBS 1X. Each data point consisted of 3/4 movies (1000 frames each); to allow the system to equilibrate a waiting step of 5 minutes was added before starting the acquisition of the first movie. Imaging was performed on a home-built TIRF microscope as previously described (26). The camera acquisition time and the excitation time were set to 250 ms; laser powers were set to 0.5 mW for both green (λ = 561 nm) and red (λ = 638 nm) lasers. The imaging buffer contained 137 mM NaCl, 2.7 mM KCl, 10 mM phosphate, 1 mM Trolox, 1% gloxy and 1% glucose. Trolox is a triplet state quencher (27, 28).

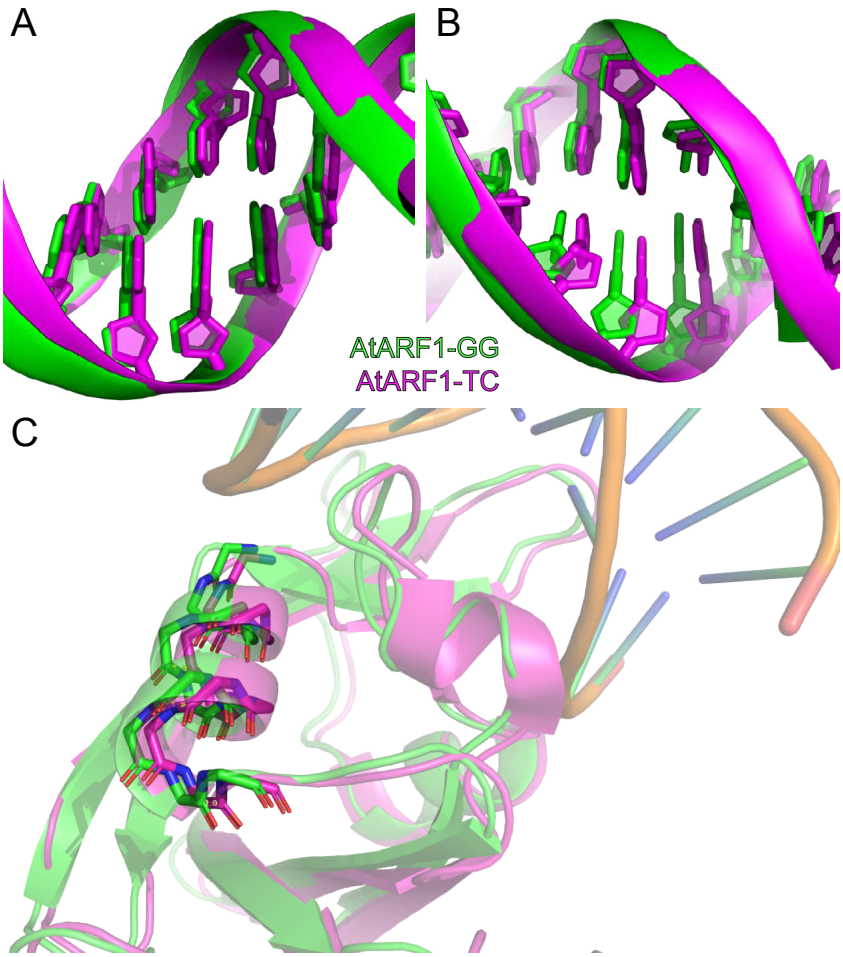

Fig. S1. Structural rearrangement of AtARF1 induced by the cognate DNA target. (A,B) Superimposition of the ARF1DBD-bound DNAs that contain TGTCGG (green) or TGTCTC (magenta). The left binding site (A) was fixed in the superposition, and the other bnding site (B) shows displacement of the DNA in the two structures. (C) Superimposition of the B3 domains of ARF1DBD in complex with TGTCGG-containing sequence (green) and that in complex with TGTCTC-containing sequence (magenta). Tighter interaction of AtARF1 with TGTCGG sequence induces a higher DNA curvature and base displacement (B), that in turn results in closer B3 subdomains (C).

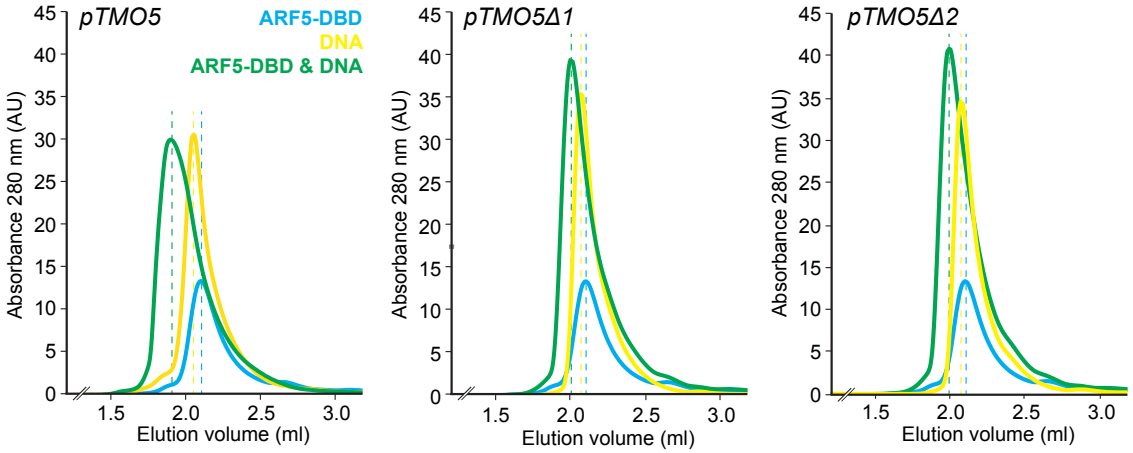

Fig. S2. Size-exclusion chromatography (SEC) traces of AtARF5-DBD with the composite AuxRE-like element in *TMO5* promoter and versions with either one (*Δ1*) or both (*Δ2*) AuxRE's mutated. Absorbance of both protein and DNA is detected at 280 nm. Note that the elution volume (in ml) of the protein with wild-type *TMO5* promoter fragment changes substantially, when compared to the shift observed with mutated *TMO5* promoter fragments.

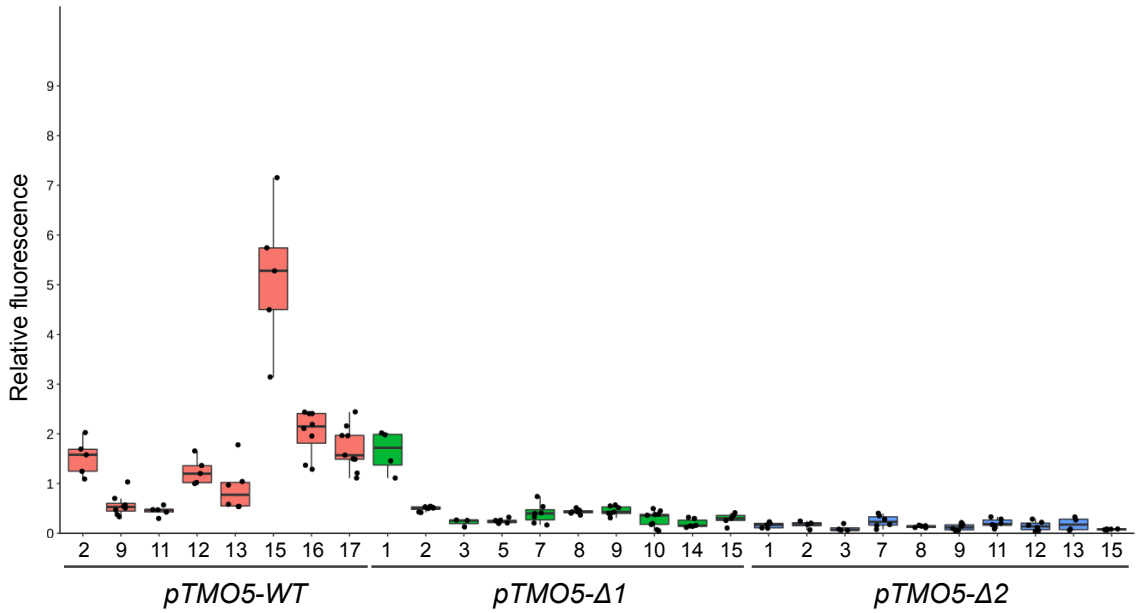

Fig. S3. Level of fluorescent signals in individual lines expressing *TMO5-3xGFP* under the control of wild-type *TMO5* promoter (*pTMO5-WT*) or the promoter in which either one (*pTMO5-Δ1*) or both (*pTMO5-Δ2*) of AuxRE-like motifs in an IR7 constellation are mutated. Box plot shows variation and the median in the mean intensities measured for individual plants. Each point is the mean GFP intensity in an individual root tip measured over the same area shown on Fig. 2C.

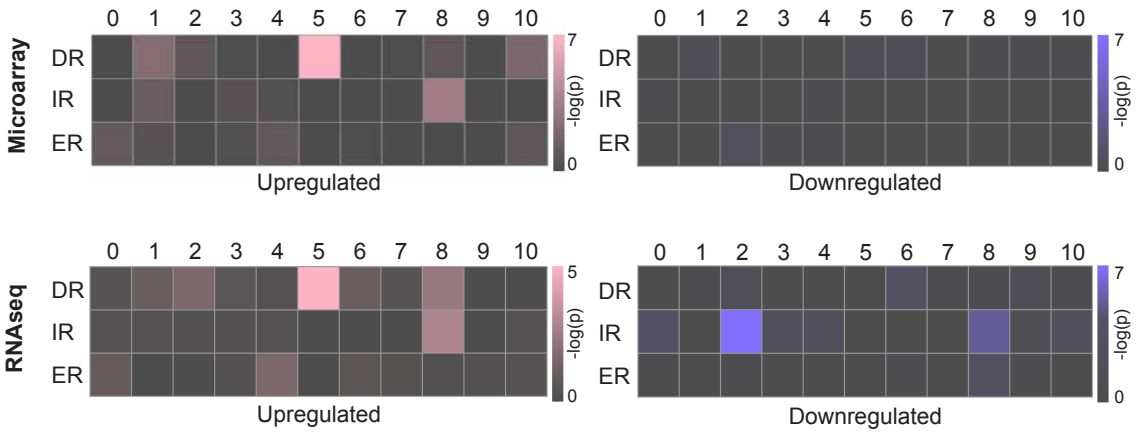

Fig. S4. Association of composite elements: direct (DR), inverted (IR) and everted repeats (ER) of TGTCNN elements, with auxin responsiveness detected in microarray datasets (top panels) and RNA-seq datasets (bottom panels). Color saturation visualizes the significance of overrepresentation for each compound element in promoters of auxin-regulated versus not-regulated genes, in –log10(meta-p-value) units. Bioinformatical analysis performed with MetaRE R package (30). The datasets used for the analysis are listed in Table S3.

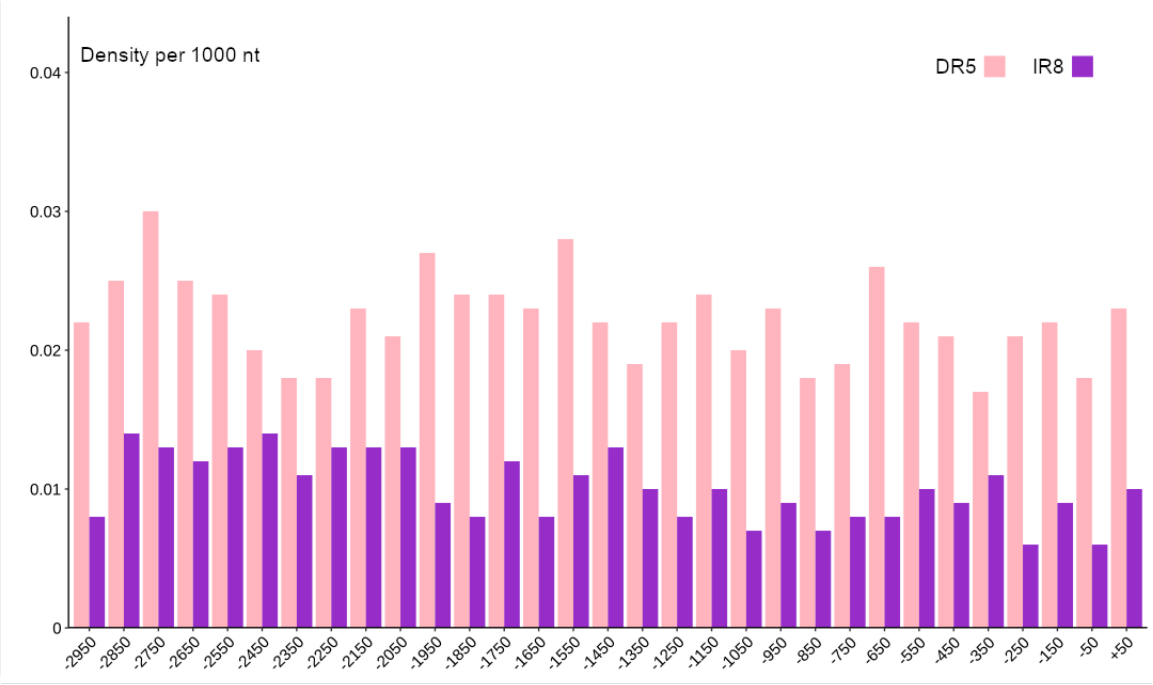

Fig. S5. Distribution of DR5 and IR8 repeats in 5' upstream regions including 5' UTR [-1500, +5'UTR] in the Arabidopsis genome. The y-axis denotes the density of repeats per 1000 nt. The x-axis denotes the 100 bp intervals in the upstream regions of all protein-coding genes. DR5 are indicated by pink color and IR8 are marked by purple color.

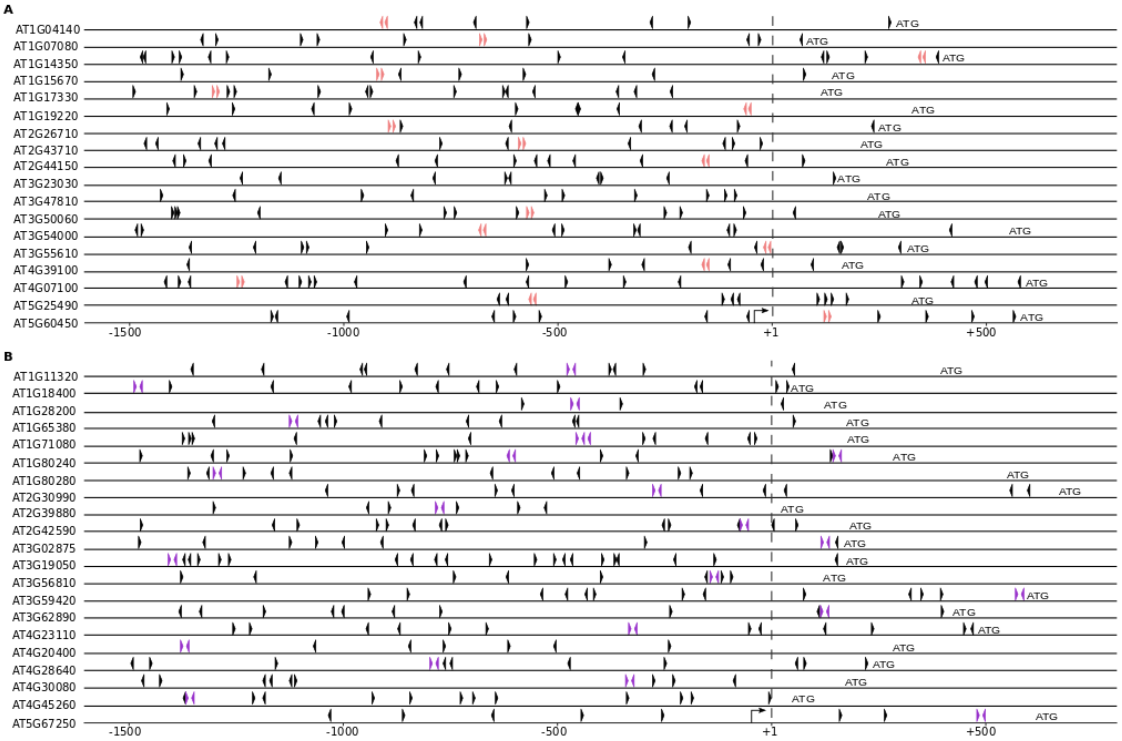

Fig. S6. Distribution of DR5 (A) and IR8 (B) repeats in 5' upstream regions of the genes tested for auxin responsiveness by qPCR. TGTC sequences shown by black triangles, those forming DR5 and IR8 repeats colored by pink and purple, correspondingly.

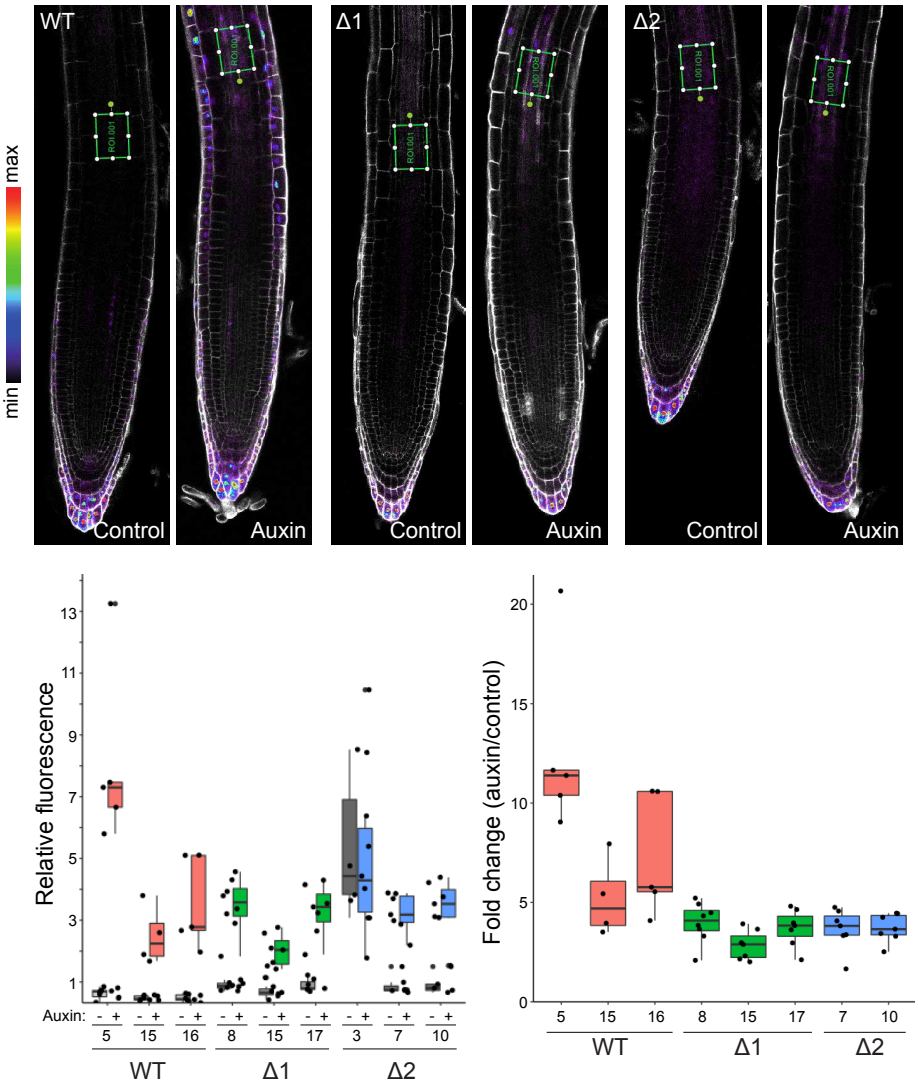

Fig. S7. (Top) Representative images of the reporter lines that express n3GFP driven by the wild-type *IAA11* promoter (*pIAA11WT*) or the *pIAA11* variant carrying mutations in one or both of the half-sites composing the IR8 element (*pIAA11Δ1* and *pIAA11Δ2* respectively). The images present five-day-old primary roots grown without hormone treatment (control) or roots treated with auxin for six-hours (Auxin). The roots were stained with propidium iodide. Green flames indicates the area used for quantification of GFP signals. (Bottom left) Levels of fluorescent signals detected in individual reporter lines expressing n3GFP driven by *pIAAWT*, *pIAA11Δ1*, or *pIAA11Δ2*. The plots indicate GFP signal intensities in 5-day-old roots grown under control condition (marked with "-") or those in roots upon auxin treatment (marked with "+"). Box plot shows variation and the median in the GFP intensities measured for individual plants. Each point is the mean GFP intensity in an individual root tip measured over the same area shown on the representative images above. (Bottom right) Summarized presentation of auxin responsiveness of individual lines. The plots indicate the ratio of GFP signal intensity in the roots upon auxin treatment to a mean GFP intensity in control condition for a specific line. Each point is the auxin response level in an individual root tip measured as GFP intensity ratio (Auxin treated versus control) over the same area shown above.

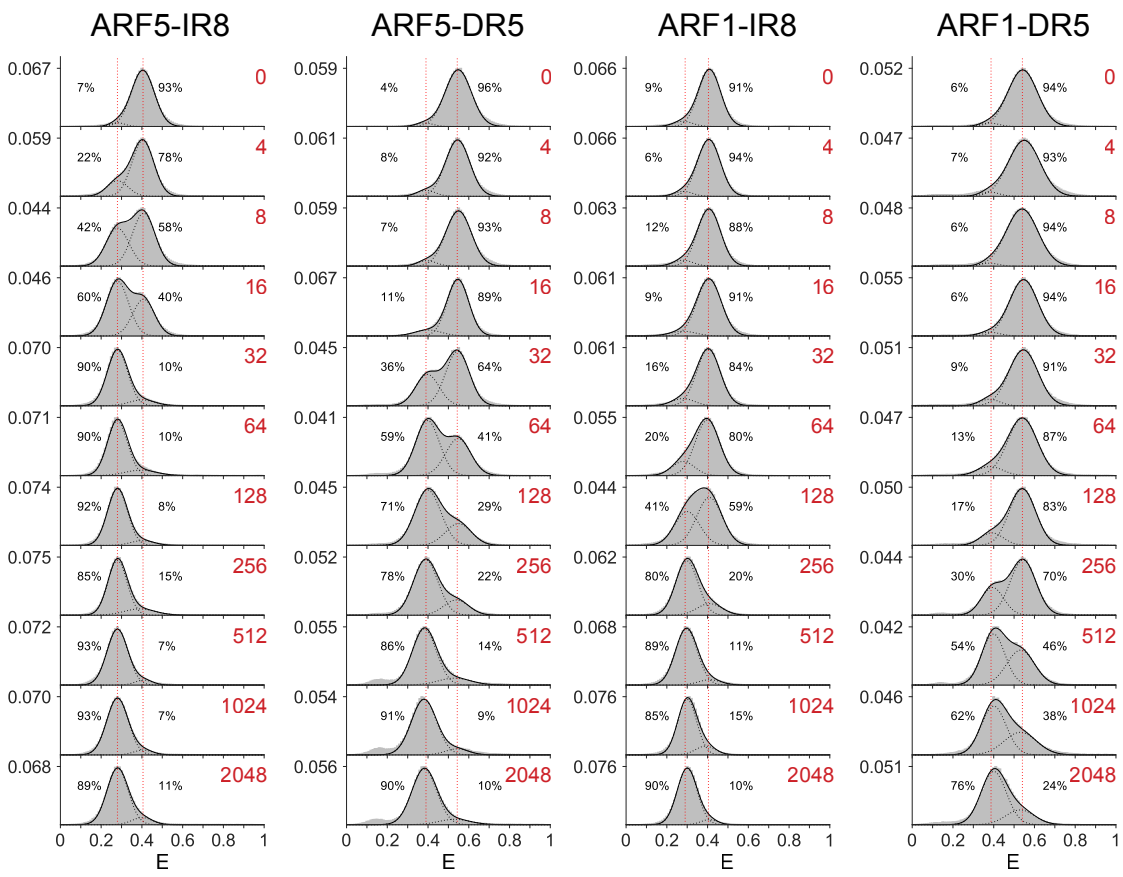

Fig. S8. Single-molecule titrations of IR8 and DR5 constructs with AtARF1-DBD and AtARF5-DBD. For each titration, the construct was immobilized on the coverslip via a neutravidin bridge and imaged using an home-built TIRF microscope. As the concentration of ARF (red number, in nM) in solution increases, the amount of ARF-bound DNA increases. We quantified the binding by fitting the FRET efficiency distributions (x-axis; E) with two Gaussians; positions (red dashed vertical lines) were fixed using values obtained from fitting the lowest and highest measured ARF concentration. The two Gaussians are shown with dashed lines in each histogram, and fraction of molecules (y-axis) in each population is given (percentages).

Table S1. Summary of the data processing and refinement statistics of the crystallographic analysis of the 6YCQ structure.

λ (Å)	0.9793	R_{cryst}[d] /R_{free}[e] (%)	0.1717 / 0.1991
Space group	$P2_1$	r.m.s.deviation from target values:	
Unit cell parameters (Å)	*a*=43.30, *b*=102.78 *c*=127.04, *β*=98.04	Bond lengths (Å)	0.008
Resolution range (Å) [a]	47.57 - 1.65 (1.680 - 1.651)	Bond angle distances (Å)	0.966
# of reflections:		Molprobity scores:	
total	257753 (269)	Clashscore (‰)	6.88
unique	75146 (268)	Poor rotamers (%)	0.16
Ellipsoidal Completeness (%)	88.1 (57.0)	Ramachandran Outliers (%)	0.15
<I / σ(I)>	15.9 (1.2)	Ramachandran Favoured (%)	97.23
Average multiplicity	3.4 (3.3)	Overall score (%)	1.52
R_{sym} (%) [b]	4.3 (80.5)	Isotropic B factor analysis	
R_{meas} (%) [b]	5.2 (99.5)	Average model B-factors (Å^2)	38.6
CC(1/2) (%)	99.9 (51.2)	B-factor from Wilson plot (Å^2)	25.97

[a] Throughout the table, the values in parentheses are for the outermost resolution shell.
[b] $R_{sym} = \Sigma_h \mid \hat{I}_h - I_{h,i} \mid / \Sigma_h \Sigma_i I_{h,i}$, where $\hat{I}_h = (1/n_h) \Sigma_i I_{h,i}$ and n_h is the number of times a reflection is measured.
[c] $R_{meas} = [\Sigma_h (n_h/[n_h-1])^{½} \Sigma_i \mid \hat{I}_h - I_{h,i} \mid] / \Sigma_h \Sigma_i I_{h,i}$, where $\hat{I}_h = (1/n_h) \Sigma_i I_{h,i}$ and n_h is the number of times a reflection is measured.
[d] $R_{cryst} = \Sigma_{hkl} \mid |F_{obs}| - k |F_{calc}| \mid / \Sigma_{hkl} |F_{obs}|$
[e] $R_{free} = \Sigma_{hkl \subset T} \mid |F_{obs}| - k |F_{calc}| \mid / \Sigma_{hkl \subset T} |F_{obs}|$ where T represents a test set comprising ~5% of all reflections excluded during refinement.

Table S2. Vascular phenotypes of wild-type Arabidopsis (Col-0), *tmo5t5l1* mutant, and the lines that under *tmo5t5l1* background carry the transgene encoding TMO5-tdT driven by the wild-type *TMO5* promoter (*pTMO5WT*) or the mutated promoters (*pTMO5Δ1*; *pTMO5Δ2*). The number of seedlings of which the primary root displayed diarch pattern are listed.

	Diarch	***N***
Col-0	12	12
tmo5 tmo5l1	0	12
***pTMO5WT* lines**		
Line 2	10	11
Line 3	9	10
Line 5	11	11
Line 7	9	9
Line 11	6	11
Line 17	10	10
***pTMO5Δ1* lines**		
Line 1	4	10
Line 6	4	11
Line 7	1	11
Line 10	0	11
Line 13	0	10
Line 15	2	11
***pTMO5Δ2* lines**		
Line 2	0	10
Line 4	3	11
Line 10	1	11
Line 13	5	10
Line 14	0	10
Line 17	4	11

Table S3. Description of auxin gene expression profiles used in the meta-analysis.

№	GEO accession	Number of DEGs		Auxin exposure		
		up	down	time	concentration and type	tissue
RNA-Seq experiments						
1	GSE149410	870	470	1h	1 μM IAA	roots
2	GSE104385[1]	1826	1381	2h	10 μM IAA	seedlings
3	GSE52966 [2]	2441	2679	4h	5 μM IAA	roots
4	GSE97258 [3]	1597	1258	6h	1 μM IAA	roots
5	GSE81166 [4]	3698	4004	55h	5 μM IBA	shoot apex explants
microarray experiments						
6	GSE35580 [5]	118	121	2h	5 μM IAA	roots
7-9	GSE42007 [6]	123	48	4h	1 μM IAA	roots
		260	139	8h	1 μM IAA	roots
		153	30	12h	1 μM IAA	roots
10-12	GSE1110 [7]	53	6	1h	0.1 μM IAA	seedlings
		215	77	1h	1 μM IAA	seedlings
		245	194	3h	1 μM IAA	seedlings
13-14	GSE42896 [8]	97	51	2h	10 μM NAA	roots
		3100	3542	6h	10 μM NAA	roots
15	GSE59426 [9]	188	80	6h	1 μM IBA	root tip

Table S4. The significance of enrichment of the TGTCNN variant repeat in upstream regions [-1500, +1] of significantly (FDR<0.05) up- and downregulated by auxin, detected by meta-analysis of ten microarray experiments (Table S3).

Variant repeat	Type	Meta p-value	
		upregulated	downregulated
TGTCNN_(N)0_TGTC	DR0	0.9943	0.9583
TGTCNN_(N)1_TGTC	DR1	3.93E-03	0.4082
TGTCNN_(N)2_TGTC	DR2	0.1469	0.9983
TGTCNN_(N)3_TGTC	DR3	0.7389	0.9534
TGTCNN_(N)4_TGTC	DR4	0.9404	0.9957
TGTCNN_(N)5_TGTC	DR5	5.91E-08	0.4415
TGTCNN_(N)6_TGTC	DR6	0.9280	0.3654
TGTCNN_(N)7_TGTC	DR7	0.7821	0.9195
TGTCNN_(N)8_TGTC	DR8	0.1452	0.5270
TGTCNN_(N)9_TGTC	DR9	0.9009	0.6124
TGTCNN_(N)10_TGTC	DR10	1.02E-02	0.7387
TGTCNN_(N)0_NNGACA	IR0	0.9251	0.7733
TGTCNN_(N)1_NNGACA	IR1	0.0666	0.9968
TGTCNN_(N)2_NNGACA	IR2	0.9759	0.7887
TGTCNN_(N)3_NNGACA	IR3	0.3342	0.7872
TGTCNN_(N)4_NNGACA	IR4	0.5679	0.5210
TGTCNN_(N)5_NNGACA	IR5	0.9597	0.8733
TGTCNN_(N)6_NNGACA	IR6	0.9997	0.9999
TGTCNN_(N)7_NNGACA	IR7	0.9775	0.9016
TGTCNN_(N)8_NNGACA	IR8	3.91E-04	0.8412
TGTCNN_(N)9_NNGACA	IR9	0.9998	0.9994
TGTCNN_(N)10_NNGACA	IR10	0.9496	0.9984
GACA_(N)0_TGTC	ER0	0.0893	0.9248
GACA_(N)1_TGTC	ER1	0.2846	0.9956
GACA_(N)2_TGTC	ER2	1.0000	0.2041
GACA_(N)3_TGTC	ER3	0.5375	0.6706
GACA_(N)4_TGTC	ER4	0.1184	0.7497
GACA_(N)5_TGTC	ER5	0.9991	0.9478
GACA_(N)6_TGTC	ER6	0.7239	0.8515
GACA_(N)7_TGTC	ER7	0.9983	0.9949
GACA_(N)8_TGTC	ER8	0.8989	0.9590
GACA_(N)9_TGTC	ER9	0.9994	0.9250
GACA_(N)10_TGTC	ER10	0.1692	0.9936

Table S5. The significance of enrichment of the TGTCNN variant repeat in upstream regions [-1500, +1] of significantly (FDR<0.05) up- and downregulated by auxin, detected by meta-analysis of five microarray experiments (Table S3).

Variant repeat	Type	Meta p-value		
		upregulated DEGs	downregulated DEGs	both up- and downregulated DEGs
TGTCNN_(N)0_TGTC	DR0	0.3098	0.9592	0.7556
TGTCNN_(N)1_TGTC	DR1	0.0580	0.6919	0.1947
TGTCNN_(N)2_TGTC	DR2	1.45E-02	0.3073	2.75E-02
TGTCNN_(N)3_TGTC	DR3	0.2407	0.9487	0.6741
TGTCNN_(N)4_TGTC	DR4	0.4074	0.8363	0.7086
TGTCNN_(N)5_TGTC	DR5	1.75E-06	0.9171	2.14E-04
TGTCNN_(N)6_TGTC	DR6	0.0515	0.1152	2.82E-02
TGTCNN_(N)7_TGTC	DR7	0.2942	0.7238	0.5295
TGTCNN_(N)8_TGTC	DR8	2.13E-03	0.6257	1.72E-02
TGTCNN_(N)9_TGTC	DR9	0.6871	0.3901	0.5878
TGTCNN_(N)10_TGTC	DR10	0.9296	0.7704	0.9494
TGTCNN_(N)0_NNGACA	IR0	0.3537	0.0829	0.1171
TGTCNN_(N)1_NNGACA	IR1	0.3568	0.9937	0.8647
TGTCNN_(N)2_NNGACA	IR2	0.5592	7.13E-03	3.46E-02
TGTCNN_(N)3_NNGACA	IR3	0.5201	0.2068	0.3173
TGTCNN_(N)4_NNGACA	IR4	0.4218	0.2530	0.3030
TGTCNN_(N)5_NNGACA	IR5	0.8682	0.8115	0.9360
TGTCNN_(N)6_NNGACA	IR6	0.8392	0.9704	0.9817
TGTCNN_(N)7_NNGACA	IR7	0.7375	0.9602	0.9568
TGTCNN_(N)8_NNGACA	IR8	4.86E-04	2.78E-02	1.28E-04
TGTCNN_(N)9_NNGACA	IR9	0.9744	0.4997	0.8934
TGTCNN_(N)10_NNGACA	IR10	0.3685	0.2427	0.2635
GACA_(N)0_TGTC	ER0	0.0793	0.8439	0.3176
GACA_(N)1_TGTC	ER1	0.9860	0.9694	0.9986
GACA_(N)2_TGTC	ER2	0.7112	0.7256	0.8229
GACA_(N)3_TGTC	ER3	0.5228	0.8053	0.7639
GACA_(N)4_TGTC	ER4	1.42E-02	0.9738	0.1839
GACA_(N)5_TGTC	ER5	0.9833	0.9085	0.9939
GACA_(N)6_TGTC	ER6	0.1855	0.6785	0.3841
GACA_(N)7_TGTC	ER7	0.4529	0.9741	0.8714
GACA_(N)8_TGTC	ER8	0.5242	0.1231	0.2280
GACA_(N)9_TGTC	ER9	0.5336	0.6833	0.6899
GACA_(N)10_TGTC	ER10	0.3282	0.9603	0.7721

Datasets:

Dataset S1 (separate file). Auxin responsiveness of IR8-containing genes analyzed by qRT-PCR. Values in the left columns are the means obtained from the ratios of log2 transformed transcript level of each gene in seedlings treated with auxin for 15 min, 1 hr, 2 hr and 6 hr to those in corresponding mock samples. The name of genes that displayed significant ($p < 0.05$) up- and downregulation are indicated in red and blue respectively. The SE of the ratios are shown in the middle columns. The right columns show the results of two-way ANOVA and one-way ANOVA with Tukey post-hoc test for comparison of the log2 transformed transcript levels of auxin-treated samples and mock samples. The analysis was conducted in two biological replicates, each with three technical replicates.

The table is uploaded as an Excel sheet.

Dataset S2 (separate file). Auxin responsiveness of DR5-containing genes analyzed by qRT-PCR. Values in the left columns are the means obtained from the ratios of log2 transformed transcript level of each gene in seedlings treated with auxin for 15 min, 1 hr, 2 hr and 6 hr to those in corresponding mock samples. The name of genes that displayed significant ($p < 0.05$) upregulation are indicated in red. The SE of the ratios are shown in the middle columns. The right columns show the results of two-way ANOVA and one-way ANOVA with Tukey post-hoc test for comparison of the log2 transformed transcript levels of auxin-treated samples and mock samples. The analysis was conducted in two biological replicates, each with three technical replicates.

The table is uploaded as an Excel sheet.

Dataset S3 (separate file). Oligonucleotides used for this study.

The table is uploaded as an Excel sheet.

SI References

1. D. R. Boer, *et al.*, Structural basis for DNA binding specificity by the auxin-dependent ARF transcription factors. *Cell* **156**, 577–589 (2014).
2. J. Juanhuix, *et al.*, Developments in optics and performance at BL13-XALOC, the macromolecular crystallography beamline at the Alba Synchrotron. *J. Synchrotron Radiat.* (2014) https:/doi.org/10.1107/S160057751400825X.
3. C. Vonrhein, *et al.*, Data processing and analysis with the autoPROC toolbox. *Acta Crystallogr. Sect. D Biol. Crystallogr.* (2011) https:/doi.org/10.1107/S0907444911007773.
4. A. J. McCoy, *et al.*, Phaser crystallographic software. *J. Appl. Crystallogr.* (2007) https:/doi.org/10.1107/S0021889807021206.
5. M. D. Winn, *et al.*, Overview of the CCP4 suite and current developments. *Acta Crystallogr. Sect. D Biol. Crystallogr.* (2011) https:/doi.org/10.1107/S0907444910045749.
6. G. N. Murshudov, *et al.*, REFMAC5 for the refinement of macromolecular crystal structures. *Acta Crystallogr. Sect. D Biol. Crystallogr.* (2011) https:/doi.org/10.1107/S0907444911001314.
7. P. Emsley, B. Lohkamp, W. G. Scott, K. Cowtan, Features and development of Coot. *Acta Crystallogr. Sect. D Biol. Crystallogr.* (2010) https:/doi.org/10.1107/S0907444910007493.
8. R. A. Laskowski, PDBsum new things. *Nucleic Acids Res.* (2009) https:/doi.org/10.1093/nar/gkn860.
9. R. C. O'Malley, *et al.*, Cistrome and Epicistrome Features Shape the Regulatory DNA Landscape. *Cell* **165**, 1280–1292 (2016).
10. F. Tian, D. C. Yang, Y. Q. Meng, J. Jin, G. Gao, PlantRegMap: charting functional regulatory maps in plants. *Nucleic Acids Res.* (2020) https:/doi.org/10.1093/nar/gkz1020.
11. A. M. Sullivan, *et al.*, Mapping and dynamics of regulatory DNA and transcription factor networks in A. thaliana. *Cell Rep.* (2014) https:/doi.org/10.1016/j.celrep.2014.08.019.
12. B. D. de Rybel, *et al.*, A versatile set of ligation-independent cloning vectors for functional studies in plants. *Plant Physiol.* **156**, 1292–1299 (2011).
13. A. Schlereth, *et al.*, MONOPTEROS controls embryonic root initiation by regulating a mobile transcription factor. *Nature* **464**, 913–916 (2010).
14. B. De Rybel, *et al.*, A bHLH Complex Controls Embryonic Vascular Tissue Establishment and Indeterminate Growth in Arabidopsis. *Dev. Cell* **24**, 426–437 (2013).
15. J. Chaiwanon, Z. Y. Wang, Spatiotemporal brassinosteroid signaling and antagonism with auxin pattern stem cell dynamics in Arabidopsis roots. *Curr. Biol.* (2015) https:/doi.org/10.1016/j.cub.2015.02.046.
16. N. A. Omelyanchuk, *et al.*, Auxin regulates functional gene groups in a fold-change-specific manner in Arabidopsis thaliana roots. *Sci. Rep.* (2017) https:/doi.org/10.1038/s41598-017-02476-8.
17. I. Mozgová, R. Muñoz-Viana, L. Hennig, PRC2 Represses Hormone-Induced Somatic Embryogenesis in Vegetative Tissue of Arabidopsis thaliana. *PLoS Genet.* (2017) https:/doi.org/10.1371/journal.pgen.1006562.
18. B. O. R. Bargmann, *et al.*, A map of cell type-specific auxin responses. *Mol. Syst. Biol.* (2013) https:/doi.org/10.1038/msb.2013.40.
19. D. R. Lewis, *et al.*, A kinetic analysis of the auxin transcriptome reveals cell wall remodeling proteins that modulate lateral root development in Arabidopsis. *Plant Cell* (2013) https:/doi.org/10.1105/tpc.113.114868.
20. J. C. Redman, B. J. Haas, G. Tanimoto, C. D. Town, Development and evaluation of an Arabidopsis whole genome Affymetrix probe array. *Plant J.* (2004) https:/doi.org/10.1111/j.1365-313X.2004.02061.x.
21. B. De Rybel, *et al.*, A role for the root cap in root branching revealed by the non-auxin probe naxillin. *Nat. Chem. Biol.* (2012) https:/doi.org/10.1038/nchembio.1044.
22. W. Xuan, *et al.*, Root cap-derived auxin pre-patterns the longitudinal axis of the arabidopsis root. *Curr. Biol.* (2015) https:/doi.org/10.1016/j.cub.2015.03.046.
23. S. Durinck, P. T. Spellman, E. Birney, W. Huber, Mapping identifiers for the integration of genomic datasets with the R/ Bioconductor package biomaRt. *Nat. Protoc.* (2009) https:/doi.org/10.1038/nprot.2009.97.

24. D. D. Novikova, P. A. Cherenkov, Y. G. Sizentsova, V. V. Mironova, metaRE R package for meta-analysis of transcriptome data to identify the cis-regulatory code behind the transcriptional reprogramming. *Genes (Basel).* (2020) https:/doi.org/10.3390/genes11060634.
25. H. Kato, *et al.*, Design principles of a minimal auxin response system. *Nat. Plants* (2020) https:/doi.org/10.1038/s41477-020-0662-y.
26. S. Farooq, J. Hohlbein, Camera-based single-molecule FRET detection with improved time resolution. *Phys. Chem. Chem. Phys.* (2015) https:/doi.org/10.1039/c5cp04137f.
27. T. Cordes, J. Vogelsang, P. Tinnefeld, On the mechanism of trolox as antiblinking and antibleaching reagent. *J. Am. Chem. Soc.* (2009) https:/doi.org/10.1021/ja809117z.
28. I. Rasnik, S. A. McKinney, T. Ha, Nonblinking and long-lasting single-molecule fluorescence imaging. *Nat. Methods* (2006) https:/doi.org/10.1038/nmeth934.